Peer-reviewed version available at *Membranes* **2017**, *7*, 45; doi:10.3390/membranes7030045

Review

Breath-Figures Self-Assembly, the Versatile Method of Manufacturing Membranes and Porous Structures: Physical, Chemical and Technological Aspects

Edward Bormashenko[a,b]

[a] Ariel University, Engineering Faculty, Department of Chemical Engineering, Biotechnology and Materials, 407000, P.O.B. 3, Ariel, Israel

[b] Tyumen State University, 6 Volodarsky St., Tyumen, 625003, Russia

Corresponding author, Edward Bormashenko, E-mail: Edward@ariel.ac.il

Abstract: The review is devoted to the physical, chemical and technological aspects of the breath-figures self-assembly process. Main stages of the process and the impact of the polymer architecture and physical parameters of the breath-figures self-assembly on the eventual pattern are covered. The review is focused on the hierarchy of spatial and temporal scales inherent for the breath-figures self-assembly. Multi-scale patterns arising from the process are addressed. The characteristic spatial lateral scales of patterns vary from nanometers to dozens of micrometers. The temporal scales of the process span from micro-seconds to seconds. The qualitative analysis performed in the paper demonstrates that the process is mainly governed by the interfacial phenomena, whereas the impact of inertia and gravity is negligible. Characterization and applications of polymer films manufactured with breath-figures self-assembly are discussed.

Keywords: membranes; polymer solution; breath-figures; ordering: capillary cluster

1. Introduction

Well-defined micro- and nano-scaled porous polymeric architectures are in a great demand for use in advanced devices, including membranes [1-4], sensors [5–6], bio-engineering [7-8] and water-oil and size-selective separation processes [9-13]. One of the most versatile, simple, single-stage and inexpensive methods, enabling manufacturing porous polymer films with finely controlled topography is the so-called "breath-figures self-assembly" [14-15]. Historically the breath figures method has been used since the 1850s by photographers as a simple and effective way to detect oil contamination on glass substrates [16]. The extended review of the numerous applications of the ordered, micro-porous films obtained with the breath-figures self-assembly may be found in Ref. 16.

The formation of water droplets on solid surfaces was first investigated by Aitken in 1893 [17] and later, in 1911, by Rayleigh [18-19]. The notion of "breath figures" refers to the set of fog droplets that forms when water vapor contacts a cold surface (solid or liquid). Breath figures are the phenomenon commonly observed in daily life. One example is the surface fog that appears on a window when we breathe on it [20]. Another example is the formation of dew [21]. Knobler and Beysens investigated the formation of breath figures under water droplets condensation [22-25] and found that they did not only form on solid surfaces but on liquids as well, specifically on paraffin oil [24]. Main features of the process breath figures self-assembly have been revealed under detailed study of water condensation in Refs. 22-25, including the intriguing effect of non-coalescence of sessile droplets, to be discussed later. The interest to the breath-figures self-assembly was revived, when Widawski, Francois, Pitois et al. demonstrated in the series of the papers [26-30], that the breath-figures self-assembly allow formation of micro-porous reliefs with well-controlled topography when polymer solutions are rapidly evaporated in a humid atmosphere. It should emphasized that in spite of the fact that the entire process looks simple, it involves almost all events inherent for interface science, namely: evaporation of a solvent, condensation of water droplets, instabilities developed in the evaporated polymer solution, delayed coalescence of closely packed droplets, and their

Peer-reviewed version available at Membranes 2017, 7, 45; doi:10.3390/membranes7030045

interaction [16]. Thus, the process of the breath-figures self-assembly may be understood only within a broad context of the surface science [31-34].

2. Impact of the Polymer Aarchitecture and Physical Parameters of the Process on the Breath-Figures Self-Assembly.

The details of the physical mechanism of the breath-figures self-assembly remains mysterious and no general mechanisms have adequately explained all experimental results [16]. It is agreed that rapid evaporation of the solvent cools the solution/humid air interface, subsequently resulting in intensive condensation of water droplets at the interface. The droplets then sink into the solution, eventually forming the honeycomb pattern, as depicted in **Figure 1**.

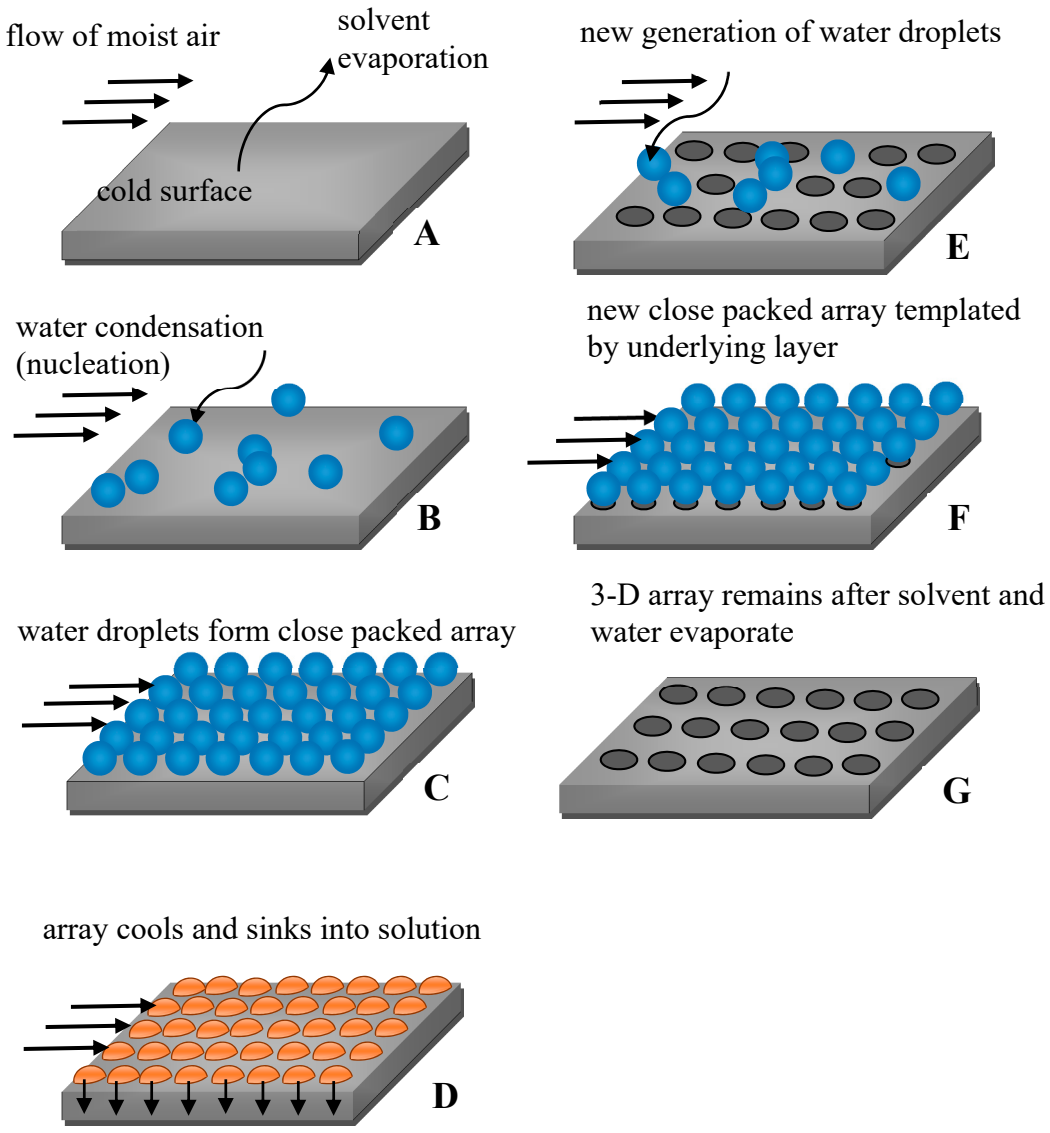

Figure 1. Sequence of stages resulting in the breath-figures self-assembly. A-D formation of the first row of pores. E-C Formation of the second row of pores.

However, the results from different researchers often seem to conflict with one other [16]. Consider first the impact of the polymer structure on the resulting patter. Bolognesi et al. reported that polar groups of polymer play a fundamental role in the process [37]. These results were supported by findings reported in Ref. 38, where the authors reported that the hydrophilic end groups can dramatically improve the film-forming property of polystyrene and that the regularity of the film is mainly influenced by the interaction of film-forming polymers with condensed water droplets. Amirkhani et al. reported that the end-functional

polymer produced a large area of regular spherical bubbles, whereas adding particles to the polymer solution leads to smaller arrays of the flattened bottom bubbles. The separation length between pores was larger for polymer/particle sample than that of the end-functional polymer films [39].

On contrary, linear polystyrene without any polar end group also led to ordered honeycomb structures when dissolved in toluene and $CHCl_3$ solvents [40-41]. At first, it was suggested that star-like and hyperbranched polymers promote formation of well-ordered structures [26, 42], however, later it was demonstrated that linear polymers also give rise to the patterns, typical for the breath-figures self-assembly, such as depicted in **Figure 2** [40-41]. It was suggested that coiled polymers (polystyrene) promote formation of breath-figures patterns [42]; on the other hand, rigid-rod conjugated polymers also gave rise to well-ordered honeycomb reliefs [36]. The impact of the molecular weight of the polymer on the resulting pattern remains obscure, and the data reported by various groups are controversial [44-46]. The concentration of the solution definitely impacts the process of the self-assembly, however its impact remains unclear [47]. The patterns, typical for breath-figures self-assembly, were obtained with amorphous [46] and crystalline polymers [48]. The additional difficulty in the identification of the impact of the polymer architecture on the resulting pattern arises from the affinity of the processes of phase separation and breath figures self-assembly giving rise to similar eventual honeycomb patterns [49].

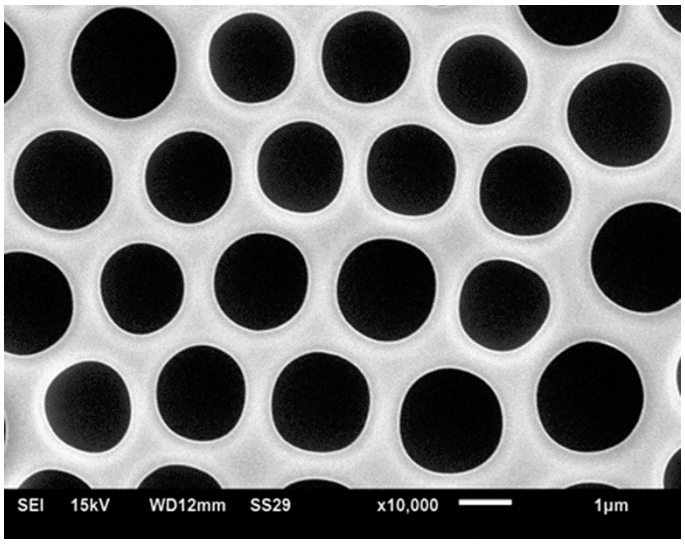

Figure 2. Typical honeycomb pattern arising from the breath-figures self-assembly. The pattern was obtained by dip-coating of the polyethylene substrate by the solution, containing 5wt.% of polycarbonate and the mixture of chlorinated solvents, namely: dichloromethane CH_2Cl_2 (90 wt.%)/chloroform $CHCl_3$ (5wt.%). The scale bar is 1 μm.

Breath-figures self-assembly has been carried out with thermoplastic [14, 15, 16, 41, 44-46] and cross-linked polymers [50-52]. Several groups reported breath-figures patterns obtained with high performance, engineering polymers, such as polyimide [53], polyetherimide [54], polysulfone [45, 55] and silicon-containing graft copolymer poly(dimethylsiloxane)-graft-polyacrylates (PDMS-g-PAs) [56].

The impact of the solvent also remains unclear. It is generally agreed that the rate of the solvent evaporation and the associated concentration and temperature dependent properties of a polymer solution define to a large extent the topography of the honeycomb pattern arising from the breath-figures process [57-58]. Ferrari et al. noted that the thermodynamic affinity between polymer and solvent is the key parameter for breath figures formation, along with other solvent characteristics such as water miscibility, boiling point and enthalpy [41]. The model predicting the evaporation profile of the casting solution in this process for low concentrations of polymer was proposed in Ref. 59. By adding a small amount of a surface active compound, it is possible to create ordered arrays also from other solvents and, thus, broaden the applicability of this patterning process markedly [60]. It was demonstrated recently experimentally that a broad diversity of solvents, including including, acetone, dichloromethane, chloroform, carbon tetrachloride, tetrahydrofuran, toluene, xylenes, carbon disulfide and N-N dimethylformamide give to

porous patterns when dissolved polystyrene and polycarbonate were evaporated in a humid atmosphere [61]. It was demonstrated that all solutions when sufficiently *pre-cooled* gave rise to typical "breath-figures" patterns [61]. Thus, the decisive factor affecting the formation of the breath-figures pattern turns out to be the temperature of the evaporated solution [16, 61].

Thus, the impact of the substrate used for the breath-figures self-assembly may be decisive due to the fact that the substrate may serve as a thermal bath stabilizing the temperature of the evaporated polymer solution, and the slide thickness is shown to be a crucial parameter in this process [59, 61-63]. However, the experimental data related to the impact of the substrate on the breath-figures self-assembly remain scarce [42, 61-62, 64-65]. Valiayaveettil and co-workers used clean glass, epoxy, amine terminated and dendrimer functionalized glass as well as silicon wafers to cast a poly(p-phenylene) with pyridine chloroform solution [65]. In this work, honeycomb membranes were obtained with glass and silicon wafers. In contrast, ring patterning, low pore density or net-type structures were obtained from the epoxy-treated, amine terminated and dendrimer functionalized glasses, respectively [65].

3. Processes Used for Breath-Figures Self-Assembly

Various experimental techniques were successfully applied for the breath figures self-assembly, including: drop-casting [66-71], spin-coating [72-78], the "doctor-blade" technique [79-80] and dip-coating [46, 54, 58, 81-83]. When breath-figures inspired patterns are formed under drop-casting a drop of polymer solution is deposited by the precise micro-syringe (or micro-injector) on the solid substrate and exposed to the air flow possessing controlled humidity [66-71]. The spin-coating process implies putting polymer solution on the center of the substrate, which is either spinning at low speed or not spinning at all. The substrate is then rotated at high speed in order to spread the evaporated polymer solution by centrifugal force. All the process is performed under controlled humidity [72-78]. In the doctor-blade technique an immobilized blade applies a unidirectional shear force to the polymer solution that passes through a small gap between the blade and the substrate [79-80, 84]. When honeycomb patterns are obtained with the dip-coating the solid substrate is pulled with a constant speed from the evaporated polymer solutions [46, 54, 58, 81-83]. In all aforementioned processes the impact of air humidity and the physico-chemical properties of a solid substrate may be decisive in the constituting the topography of the resulting honeycomb relief [14-16, 59, 64, 67].

4. Main Stages of the Breath-Figures Self-Assembly.

Main stages of breath-figures include: nucleation of water droplets, condensation on the polymer solution/vapor interface, interaction between droplets and final removal of water and its evaporation. Condensation is a process of the formation of a liquid phase from the gaseous (vapor) one, which starts from "nucleation". Nucleation is the formation of an embryo or nucleus of a new phase in another phase [32, 85]. Homogeneous and heterogeneous nucleation scenarios should be distinguished. Heterogeneous nucleation takes place in the presence of foreign particles or surfaces, whereas the homogeneous nucleation occurs under forming and growing small clusters of molecules [86]. If it is thermodynamically favorable for these clusters to grow they become recognizable droplets of the liquid phase [32, 85-86]. It should be emphasized that the precise mechanism of nucleation under the breath-figures self-assembly remains unclear, due to the fact that nuclei of water droplets are formed in the presence of solvent vapor [87]. The processes of nucleation and condensation have a decisive influence on the formation of the eventual breath-figures-inspired pattern [87], hence additional experimental and theoretical efforts are necessary for elucidating the kinetics of nucleation and condensation taking place under the conditions of the breath-figures self-assembly.

It is also possible that nucleation occurs at the polymer solution/vapor interface. In this case the nucleation rate I (for its accurate definition, see Refs. 32, 88-91) is modified through the function depending strongly on the equilibrium (Young) contact angle θ_Y, namely: $I \approx \exp\left(-\frac{\Delta G^{het}_{\max}(\theta_Y)}{k_B T}\right)$, where $\Delta G^{het}_{\max}$ is the value of the potential barrier to be surmounted for heterogeneous nucleation, T is the temperature and k_B is the Boltzmann constant. The value of $\Delta G^{het}_{\max}$ for a contact angle hysteresis free substrate is given by:

$$\Delta G_{\max}^{het}(\theta_Y) = \Delta G_{\max}^{\hom} \frac{(2+\cos\theta_Y)(1-\cos\theta_Y)^2}{4}, \quad (1)$$

where $\Delta G_{\max}^{\hom}$ is the potential barrier of the homogeneous nucleation supplied by Eq. (2).

$$\Delta G_{\max}^{\hom} = \frac{\gamma 4\pi r_c^2}{3}, \quad (2)$$

where r_c is the size of the critical nucleus and γ is the surface tension [86, 88].

Beysens et al. studied the formation of breath figures patterns formed on cold borosilicate substrates, either pristine or hydrophobized by the solution of octadecyltrichlorosilane [22]. The treatment by octadecyltrichlorosilane enabled to control of the apparent contact angle of the cooled solid substrate [22]. The pattern for water on glass was studied by direct observation and light scattering as a function of the contact angle θ_Y, the velocity of vapor volume transfer "flux", denoted Φ_{vol}, degree of supersaturation ΔT and time *t*. It was established that when $\theta_Y = 0^0$, a uniform water layer forms whose thickness grows as *t* at constant Φ_{vol} and ΔT. For $\theta_Y = 90^0$, droplets are formed at constant Φ_{vol} and ΔT; the radius of an isolated droplet grows as $t^{0.23}$, but as a result of coa1escences the average droplet radius grows as $t^{0.75}$ [22]. The most important conclusion following from these considerations is well-expectable, namely the condensation "breath-figures" pattern depends on the apparent contact angle θ_Y, as predicted by Eqs. 1-2. The growth process is accompanied with coalescence of droplets and it turned out to be self-similar; coalescences simply rescaled the distances and left the basic droplet pattern unaltered [22]. The details of the coalescence were addressed in Ref. 23; the authors shown that the number of coalescences undergone by a given droplet grows logarithmically with time; the total distance traveled by this droplet is proportional to its size [23]. The experiments, reported by Beysens et al., supported the important information about the kinetics of formation of the "breath-figures" patterns [22-23]. However, these experiments have been carried under model conditions in the absence of evaporated polymer solution, which complicates the physics of the process essentially; hence, novel experimental data shedding light on the kinetics of formation of breath-figures patterns occurring at the polymer solution/vapor interface are necessary.

5. Multi-Scale Patterning Observed Under the "Breath-Figures Self-Assembly"

Multi-scale, hierarchical patterning features the breath-figures self-assembly [14, 76-77, 93-94]. The characteristic spatial scales of patterns vary from nanometers to dozens of micrometers. Consider the large-scale patterning observed in rapidly evaporated polymer solutions [94-99], depicted in **Figure 3**, observed under the dip-coating of substrates with rapidly evaporated polymer solutions (similar large-scale patterns were observed also under other experimental techniques [96-99]). In particular, it was demonstrated that the characteristic dimension of cells constituting the pattern grow with the concentration of the polymer solution [95].

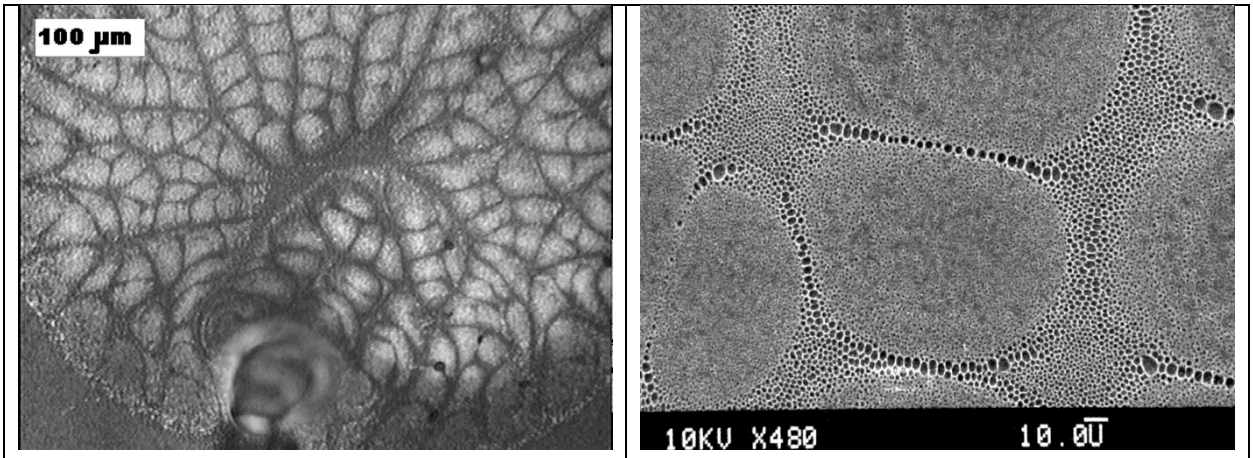

Figure 3. Large-scale pattern typical for the breath-figures self-assembly (Polystyrene (5wt.%) was dissolved in a mixture of dichloromethane CH_2Cl_2 (90 wt.%) and chloroform $CHCl_3$ (5wt.%) and deposited by dip-coating on the polyethylene substrate).

The physical mechanism of the patterning remains debatable. For film thickness less than about 100 nm (thin layers) effective molecular interactions between the liquid layer surface and the substrate dominate all other forces (like thermo- or soluto-capillarity or gravity) and thus determine the film stability and patterning under dewetting [100–102].

For evaporated films of a thickness above 100 nm thermo-capillarity forces become dominant, resulting in instability caused by the Marangoni convection, either thermo- or soluto-capillary [103-113]. It should be mentioned that the analysis of the thermo- and soluto-capillarity inspired patterning in essentially non-linear one and involves complicated mathematical models [103-108]. It was demonstrated experimentally that the patterns observed in the evaporated (cooled from above) layers are different from those, formed in the layer heated from below without evaporation [109]. Thus, the kinetics of evaporation, studied in Ref. 110, turns out to be crucial for constituting large-scale patterns. The apparatus, utilizing self-organized liquid flow for the targeted modification of macromolecular systems in a solution was suggested in Ref. 112. Marangoni-flows-induced patterns, observed under spin-coating of evaporated polymer solutions were reported in Ref. 114. When the polymer solution is evaporated, the thermo- and soluto-capillary flows occur and both of them may contribute to the eventual patterning, and it remains disputable to decide, what of Marangoni flows has a decisive impact on the patterning. The experimental data reported in Refs. 95, 115 convince, that this is the solutal Marangoni flow, which constitutes the pattern. Indeed, heating the substrate from below destroyed the patterning [115]. This contradicts the idea that self-organization is due to the jump in surface tension caused by a temperature gradient (temperature-gradient-driven Marangoni instability).

However, when evaporation is present thermo- and soluto-capillarity represents only one of several destabilizing mechanisms: vapor recoil, differential evaporation (dependence of the evaporation rate on the thickness of the film) and, sometimes, all contribute to the development of interfacial instability and as a result exert an influence on the pattern's makeup [116]. De Gennes proposed an alternative mechanism of patterning. He has shown that in an evaporating film, a "plume" of solvent-rich fluid induces a local depression in surface tension, and the surface forces tend to strengthen the plume. His calculations led to the conclusion that this kind of instability should dominate over the classic Bénard–Marangoni instabilities [117-118]. It should be emphasized that in all kinds of aforementioned instabilities (namely Marangoni and de Gennes ones) the tangential vector field of velocities drives the liquid. This makes possible the topologically-based approach to patterning as demonstrated in Ref. 119. The "hairy ball theorem" of algebraic topology states that any continuous tangent vector film on the surface topologically equivalent to a sphere must have at least one point where the vector is zero [120]. Remarkably, the "hairy ball theorem"

predicts the existence of at least one zero tangential velocity point at the surface of the evaporated polymer solution [119]. And, indeed, these zero velocity points were observed experimentally [119].

What is the role of water droplets in the formation of large scale patterns, shown in **Figure 3**? It seems that water droplets work as "tracers" enabling visualization of the boundaries, separating the large scale cells, depicted in **Figure 3**. Pores, appearing after droplets evaporation are accumulated in zero-velocity points, arising from the "hairy ball theorem", as discussed in Refs. 119-121.

Now consider mesoscopic, micro-scaled patterning observed by various groups [14-16, 26-30, 35-36, 53, 67-6]. These mesoscopic patterns are built from well-ordered micro-scaled or sub-micro-scaled pores, demonstrating long-range 2D and sometimes 3D ordering [35, 122-124]. The mechanism of this patterning was discussed in Refs 48 and 66. Govor et al. related the mesoscopic ordering to capillary interaction between droplets, discussed in much detail in Refs. 125-128. Kralchevsky et al. demonstrated that between two particles placed on the liquid/vapor interface acts the force (which may be either attractive or repulsive), similar to the Coulomb interaction between two endless wires, charged with the constant linear charge densities [125-128]. It is reasonable to suggest that this capillary interaction between droplets, condensed at the polymer solution/humid vapor interface is responsible for the long-range ordering inherent for the breath-figures self-assembly. It was already demonstrated by Bragg, Nye and Lomer in Refs. 129-130, that the capillary interaction of bubbles promotes assemblage of bubbles, representing the crystal structure of real metals.

Capillary interaction is not the only kind of physical interactions acting between particles, placed at the liquid/vapor interface. It was demonstrated by Pieranski that electrostatic interactions between floating particles may be not less important than capillary ones [131]. The role of the Marangoni thermo-capillary convection in the formation of ordered honeycomb patterns was mentioned in Refs. 66, 132-133. The details of the physical mechanism giving rise to the long-range self-assembly of pores, inherent for the breath-figures patterning remain unclear. It is noteworthy that the formation of ordered ensembles of droplets under drop casting method occurs in the vicinity of the triple (three-phase) line, as shown in **Figure 4** [134]. Self-assembly of colloidal particles (not droplets!) taking place in the vicinity of the triple line was studied extensively in Refs. 135-136. However, the approach developed in Refs. 135-136 hardly could be extended to the explanation of the self-assembly of condensed water droplets, due to their coalescence to be discussed below.

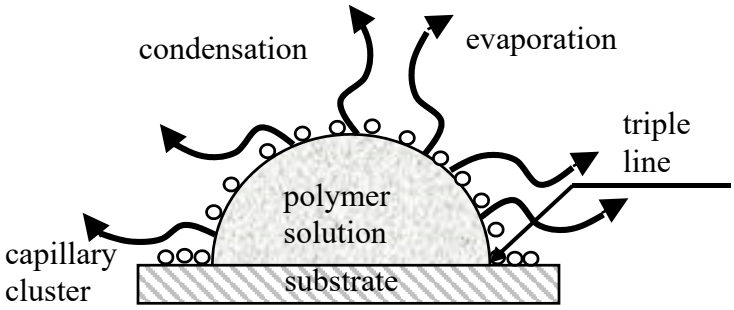

Figure 4. Breath figures self-assembly taking place under drop casting is depicted. The droplet of the polymer solution is evaporated in the humid atmosphere. Water droplets are condensed at the polymer solution/vapor interface. The capillary cluster built from water droplets is formed in the vicinity of the triple (three-phase line).

It was also demonstrated that some additives such as PEG and dendrons promote ordering occurring under the breath-figures self-assembly [62, 137-138]. The well-ordered honeycomb patterns resulting from the breath-figures self-assembly evidences non-coalescence or delayed coalescence of sessile water droplets condensed on the polymer solution/vapor interface. This means that so-called "capillary cluster" built from micro-scaled water droplets exists on the polymer solution/vapor interface. The physical behavior of non-

coalescence capillary clusters, in which capillary interactions prevail or play essential role draw an attention of investigators recently [139-141].

When droplets of the same liquid touch one another one expects coalescence [23, 142-143]. The mechanism of the non-coalescence, observed in capillary clusters, remains disputable. Karpitschka et al. showed that sessile droplets from different but completely miscible liquids do not always coalesce instantaneously upon contact: the drop bodies remain separated in a temporary state of non-coalescence, connected through a thin liquid bridge [144-146]. Karpitschka et al. suggested that the delay originates from the Marangoni convection [144-146]. However, the details of the non-coalescence of droplets in capillary clusters remain unclear and call for further experimental and theoretical insights.

Nanoparticles also prevent coalescence of droplets and enable the formation of the additional nanoscale in the hierarchical topographies obtained under the breath-figures self-assembly (see the extended review of the state of art use of nano-particles in the breath-figures self-assembly in ref. 16 and Refs. 147-150. Saunders et al. demonstrated that the super-lattice of mono-dispersed gold nanocrystals formed under the breath-figures process an ordered structure at the nanometer scale [150]. An interaction between the nano- and the micro-meter length scale self-organization processes, especially through the formation of water droplets/evaporating polymer solution interface and droplet collective motions was addressed in Ref. 151.

Now consider the dimensionless numbers, describing the breath–figures self-assembly, namely the Bond (*Bo*), capillary (*Ca*) and Reynolds (*Re*) numbers:

$$Bo = \frac{\rho g L^2}{\gamma},\ Ca = \frac{\eta v}{\gamma},\ \mathrm{Re} = \frac{\rho v L}{\gamma}, \tag{3}$$

where ρ is the density (the densities of water and polymer solutions are very close), η and γ are the viscosity and surface tension of the polymer solution respectively, v is the characteristic velocity of droplets and pores and L as the characteristic spatial scale.

Assuming for numerical values of physical parameters appearing in Eqs. 3: $\rho \cong 1.0\times 10^3 \frac{kg}{m^3}; \gamma \cong 25\times 10^{-3}\frac{J}{m^2}; \eta \cong 10^{-2} - 10^{-1} Pa\times s; v \cong 10-30\frac{\mu m}{S}$ (the viscosity of the solution is taken for the initial stage of the evaporation, the velocity equals to the maximal velocity of pores, established experimentally in Ref. 121); we conclude, that inequalities:

$$Bo << 1,\ Ca << 1,\ \mathrm{Re} << 1 \tag{4}$$

take place for all lateral characteristic scale lengths, inherent for the breath-figures self-assembly, namely: $10^{-9} m < L < 10^{-5} m$. This means that the effects due to gravity, inertia and viscosity are negligible, and the breath figures self-assembly is mainly driven by the interfacial phenomena (however, the viscosity, growing with the evaporation of the polymer solution layer, helps to stabilize the eventual honeycomb pattern, as it will be shown below). Indeed, the breath figures patterns were observed on horizontal [14-16] and vertical [46, 95-97] substrates. It is seen from Eqations 4, that the breath-figures self-assembly is a "slow" process, in which effects due to inertia and viscosity are negligible.

In order to clarify the precise meaning of the wording "slow process" it is instructive to elucidate the hierarchy of time scales, inherent for the process, namely: τ_{therm}^{sol} and τ_{therm}^{drop} which are the characteristic times necessary for attaining thermal equilibrium in the evaporated polymer solution and condensed water droplets respectively, $\tau_{\mathrm{int}erf/visc}$, which is the characteristic time necessary for viscous stresses (developed in the evaporated polymer solution layer) for balancing interfacial ones (at the length scale of a single droplet R), and eventually the temporal scales $\tau_{ev}^{sol} \cong 10s$ and $\tau_{ev}^{drop} \cong 1s$ which are the characteristic times of evaporation of the polymer solution and water droplets, correspondingly. The estimations for the time scales yield:

$$\tau_{therm}^{sol} \cong \frac{L_{sol}^2}{\alpha_{sol}}; \tau_{therm}^{drop} \cong \frac{R^2}{\alpha_w}; \tau_{\mathrm{int}erf/visc} \cong \frac{\eta R}{\gamma}, \tag{5}$$

where α_{sol} and α_w are the thermal diffusivities of a polymer solution and water respectively, L_{sol} and R are the characteristic spatial scales of the evaporated layer of the polymer solution (in other words its typical thickness) and the condensed droplet (i.e. its radius), correspondingly; η and γ are the viscosity and the surface tension of the polymer solution at the initial stage of the evaporation, as noted above.

Assuming: $\alpha_{sol} \cong 7.7 \times 10^{-8} \frac{m^2}{s}$ (as it is taken for the chloroform, as a typical solvent); $\alpha_w \cong 1.47 \times 10^{-7} \frac{m^2}{s}, L_{sol} \cong 10^{-4} m, R \cong 10^{-6} m$, yields following rough estimations: $\tau_{therm}^{sol} \cong 0.13 s; \tau_{therm}^{drop} \cong 7 \times 10^{-6} s; \tau_{\text{int}erf/visc} \cong 0.5 \times (10^{-5} - 10^{-6}) s$.

Finally, we estimate the hierarchy of time scales inherent for the breath-figures self-assembly:

$$\tau_{ev}^{sol} > \tau_{ev}^{drop} \geq \tau_{therm}^{sol} >> \tau_{therm}^{drop} \geq \tau_{\text{int}erf/visc} \quad (6)$$

This hierarchy may be interpreted as follows: the condensed water droplet practically immediately comes to the thermal equilibrium, whereas the polymer solution layer, fixing the pattern, is far from the thermal equilibrium on the time scale of its evaporation. The Inequality (6) also implies that at the lateral scale of a single droplet interfacial stresses are immediately balanced by viscous ones, which are developed in the polymer solution layer. So, the behavior of a single droplet is quasi-static, and the formation of pores is stabilized by the viscosity of polymer layer, growing with the evaporation; whereas the, dynamics and thermodynamics of large (~ 10 μm) cells, depicted in **Figure 3**, are essentially non-equilibrium.

6. Characterization of Patterns, Obtained with the Breath-Figures Self-Assembly.

6.1. Characterization of Ordering of Patterns.

Ordered honeycomb structures arise from the breath-figures self-assembly. How the 2D ordering of patterns may be quantified? Two approaches to the quantifying of surface ordering have been reported; the first of which exploited the statistical properties of the auto-correlation functions [152], calculated over pixels of the SEM images taken for honeycomb patterns [62]. The correlational analysis of the SEM images indicated short-range and mesoscopic ordering of the honeycomb structures on the characteristic scale of 5 μm for the typical, weakly ordered patterns, represented in Figure 2. The second approach to the problem involved the use of the Voronoi diagrams (or the Voronoi tessellations) described in detail in Refs. 153-154. Perfect ordering of pores on the scale of 1-10 mm was registered [14-16]. The Voronoi tessellation and Voronoi entropy were successfully applied for the quantitative characterization of ordering of capillary clusters (see Ref. 141) and pores constituting honeycomb reliefs in Refs. 73, 155-156.

6.2. Surface Characterization of Patterns, Obtained with the Breath-Figures Self-Assembly.

The simplest and extremely useful method of characterization of micro-rough surfaces is based on the measurement of the apparent contact angle [32-34, 157]. The detailed study of the apparent contact angles inherent for honeycomb, porous surfaces arising from the breath-figures self-assembly was reported in Refs. 158-160. It was demonstrated that honeycomb surfaces produced by the breath figures self-assembly demonstrate the pronounced heterogeneous (air trapping) Cassie-Baxter wetting regime [79, 161-163]. The interfaces characterized by the stable Cassie-Baxter wetting are featured by high apparent contact angles and low contact angle hysteresis [32-34, 161-163]. Thus, they are suitable for a broad range of applications, where self-cleaning properties of the interface are demanded [164-165]. Somewhat surprisingly, polymer surfaces manufactured with the breath-figures self-assembly shown the Cassie-like wetting, even when hydrophilized by metal coating [160]. The mechanism of stability of the Cassie wetting states observed on honeycomb polymer and metallized reliefs was addressed in Ref. 166.

At the same time the mechanical properties of micro-porous films, obtained with the breath-figures self-assembly, remain obscure. The non-trivial mechanical properties of these films, possessing reduced size and dimensionality, are expected, as compared with those of their macroscopic counterparts [167].

7. Novel Applications of the Breath-Figures Self-Assembly.

We already considered the numerous applications of interfacial honeycomb structures, arising from the breath-figures self-assembly in Section 1 (see also the comprehensive review presented in Ref. 16). A number of very recent applications of these structures are noteworthy. Microporous functional polymer surfaces, arising from the breath-figures self-assembly have been proven to be selective surfaces toward eukaryotic cells while maintaining antifouling properties against bacteria [168]. The witty process of manufacturing of micro-spherical particles with the breath-figures process was reported in Ref. 169. Breath-figures self-assembly was successfully involved in manufacturing solid-state supercapacitors [170]. It was shown, that honeycomb polymer films supported by steel meshes enable manufacturing electrically controlled membranes [171].

8 Conclusions

Breath-figures self-assembly enables manufacturing micro- and sub-micro scaled porous reliefs demonstrating a potential for manufacturing membranes, functionalized templates, sensors, optical and bio-engineering devices and water-oil and size-selective separation processes [16]. Breath-figures inspired topographies may be obtained with thermoplastic [14, 15, 16, 37-38, 41, 44-46, 61-62] and thermosetting [50-52] polymers. High-performance engineering polymers, such as polyimide [53], polyetherimide [54] and polysulfone [45,55] were successfully used for the breath-figures self-assembly. 2D and 3D hierarchical structures, possessing a range of scales from micro-meters to nano-meters were reported [14, 35, 150]. The nature of the large-scale (~ 10 μm) patterning, attributed by different authors to various kinds of hydrodynamic instabilities remains disputable [95-98, 117-118].

The breath figures self-assembly is a robust, single-stage process, however, it involves almost all events inherent for interface science, namely: evaporation of a solvent, condensation of water droplets, instabilities developed in the evaporated polymer solution, delayed coalescence of closely packed droplets, forming the capillary cluster and their interaction [16, 125-131]. Thus, the process of the breath-figures self-assembly may be understood only within a broad context of the surface science [31-34].

A variety of basic questions related to the physical and chemical mechanisms of the breath-figures self-assembly remains obscure; even the impact of the polymer architecture on the resulting pattern is unclear and calls for future investigations. In this situation the qualitative macroscopic approach to the analysis of the process becomes preferable. Such an analysis is proposed in the review. The estimation of dimensionless numbers, describing the breath–figures self-assembly, namely the Bond (*Bo*), capillary (*Ca*) and Reynolds (*Re*) numbers, convinces that the effects due to gravity, inertia and viscosity are negligible, at least at the first stage of evaporation of a polymer solution, and the process is mainly driven by the interfacial phenomena. The viscosity of a polymer layer contributes to the stabilization of the pores radii.

The hierarchy of spatial and temporal scales inherent for the breath-figures self-assembly is elucidated. The characteristic spatial scales of patterns range from dozens of micrometers to nanometers. The temporal scales of the process vary from micro-seconds to seconds. The analysis of the hierarchy of temporal scales demonstrates that the condensed water droplet practically immediately comes to the thermal equilibrium, whereas the polymer solution layer is far from the thermal equilibrium. It is also-shown that the behavior of a single droplet is quasi-static; whereas the dynamics and thermodynamics of large-scale cells are essentially non-equilibrium. The topological aspect of the self-assembly is addressed [119].

The novel applications and trends of future investigations in the field of the breath-figures self-assembly are envisaged.

Acknowledgements: The author is thankful to Mrs. Yelena Bormashenko for her kind help in preparing this manuscript.

References

1. Gugliuzza, A.; Aceto, M.C.; Macedonio, F.; Drioli, E. Water droplets as template for next generation self-assembled poly-(etheretherketone) with Cardo membranes. *J. Phys. Chem. B* **2008**, *112*, 10483–10496.
2. Ulbricht, M. Advanced functional polymer membranes. *Polymer* **2006**, *47*, 2217–2262.

3. Schechter, A.; Savinell, R. F. Imidazole and 1-methyl imidazole in phosphoric acid doped polybenzimidazole, electrolyte for fuel cells. *Solid State Ionics* **2002**, *147*, 181–187.
4. Gugliuzza, A.; Perrotta, M. L.; Drioli E. Controlled bulk properties of composite polymeric solutions for extensive structural order of honeycomb polysulfone membranes. *Membranes* **2016**, *6*, 27.
5. Yang, J.-Sh.; Swager, T. M. Fluorescent porous polymer films as TNT chemosensors: electronic and structural effects. *J. Am. Chem. Soc*. **1998**, *120*, 11864-11873.
6. Li, Y. T.; Cunin, Fr.; Link, J. R.; Gao, T.; Betts, R. T.; Reiver, S. H, Chin, V. Polymer replicas of photonic porous silicon for sensing and drug delivery applications. *Science* **2003**, *299 (5615)*, 2045-2047.
7. Rezwan, R.; Chen, Q. Z.; Blaker, J. J.; Boccaccini A. R. Biodegradable and bioactive porous polymer/inorganic composite scaffolds for bone tissue engineering. *Biomaterials* **2006**, *27*, 3413–3431.
8. Lin, A. S. P.; Barrows, Th. H.; Cartmell, S. H.; Guldberg, R. E. Microarchitectural and mechanical characterization of oriented porous polymer scaffolds. *Biomaterials* **2003**, *24*, 481–489.
9. Li, H.; Zhao, X.; Wu, P.; Zhang, Sh.; Geng, B. Facile preparation of superhydrophobic and superoleophilic porous polymer membranes for oil/water separation from a polyarylester polydimethylsiloxane block copolymer. *J. Materials Sci*. **2016**, *51*, 3211–3218.
10. Cheng, B.; Lib, Z.; Li, Q.; Ju, J.; Kang, W.; Naebe, M. Development of smart poly(vinylidene fluoride)-graft-poly(acrylic acid) tree-like nanofiber membrane for pH-responsive oil/water separation. *J. Membrane Sci*. **2017**, *534*, 1–8.
11. Bormashenko, Ed.; Balter, S.; Bormashenko, Ye.; Aurbach, D. Honeycomb structures obtained with breath figures self-assembly allow water/oil separation. *Colloids and Surfaces A* **2012**, *415*, 394–398.
12. Liu, C.; Yang, J.; Tang, Y.; Yin, L.; Tang, H.; Li, Ch. Versatile fabrication of the magnetic polymer-based graphene foam and applications for oil–water separation. *Colloids and Surfaces A* **2015**, *468*, 10–16.
13. Wan, L.-S.; Li, J.W.; Ke, B-B.; Xu, Z-K. Ordered microporous membranes templated by breath figures for size-selective separation. *J. Am. Chem. Soc*. **2012**, *134*, 95–98.
14. Muñoz-Bonilla, A. Fernández-García, M.; Hernández, J. R. Towards hierarchically ordered functional porous polymeric surfaces prepared by the breath figures approach. *Progress Polymer Sci.* **2014**, *39*, 510–554.
15. Bunz, U. H. F. Breath figures as a dynamic templating method for polymers and nanomaterials. *Advanced Mater*. **2006**, *18*, 973–989.
16. Zhang, A.; Bai, H.; Li, L. Breath Figure: A Nature-inspired preparation method for ordered porous films. *Chem. Rev*. **2015**, *115*, 9801−9868.
17. Aitken, J. Breath figures. *Nature* **1911**, *86*, 516-617.
18. L. Rayleigh, Breath figures. *Nature* **1911**, *86*, 416-417.
19. L. Rayleigh, Breath figures. *Nature* **1912**, *90*, 436-438.
20. Briscoe, B.; Galvin, K. The effect of surface fog on the transmittance of light. *J. Sol. Energy* **1991**, *46*, 191-197.
21. Beysens, D. The formation of dew. *Atmospheric Research* **1995**, *39*, 215-237.
22. Beysens, D.; Knobler C. M. Growth of breath figures. *Phys. Rev. Lett*. **1986**, *57*, 1433- 1436.
23. Marcos-Martin, M.; Beysens, D.; Bouchaud, J. P.; Godrèche, C.; Yekutieli, I. Self-diffusion and 'visited' surface in the droplet condensation problem (breath figures). *Physica A* **1995**, *214*, 396-412.
24. Knobler, C. M.; Beysens, D. Growth of breath figures on fluid surfaces. *Europhys. Lett*. **1988,** *6*, 707.
25. Steyer, A.; Guenoun, P.; Beysens, D.; Knobler, C. M. Two-dimensional ordering during droplet growth on a liquid surface. *Phys. Rev. B* **1990**, *42*, 1086.
26. Widawski, G.; Rawiso, B.; Francois, B. Self-organized honeycomb morphology of star-polymer polystyrene films. *Nature* **1994**, *369*, 387-389.
27. Francois, B.; Pitois, O.; Francois, J. Polymer films with a self- organized honeycomb morphology. *Adv. Mater*. **1995**, *7*, 1041-1044.
28. Pitois, O.; Francois, B. Formation of ordered micro-porous membranes. *Eur. Phys. J. B* **1999**, *8*, 225-231.
29. Pitois O.; François, B. Crystallization of condensation droplets on a liquid surface *Colloid & Polymer Sci.* **1999**, *277*, 574–578

30. François, B.; Ederlé, Y, Mathis, C. Honeycomb membranes made from $C_{60}(PS)_6$. *Synthetic Metals* **1999**, *103*, 2362-2363.
31. Adamson, A. W., Gast A. P. *Physical Chemistry of Surfaces*, Sixth Edition, Wiley-Interscience Publishers, New York, 1990.
32. Erbil H. Y. *Surface Chemistry of Solid and Liquid Interfaces*, Blackwell, Oxford, 2006.
33. de Gennes P. G.; Brochard-Wyart F.; Quéré D. *Capillarity and Wetting Phenomena*, Springer, Berlin, 2003.
34. Bormashenko, Ed. *Wetting of real surfaces*, De Gruyter, Berlin, 2013.
35. Srinivasarao, M.; Collings, D.; Philips, A.; Patel, S. Three-dimensionally ordered array of air bubbles in a polymer film. *Science* **2001**, *292*, 79-83.
36. Song, L.; Bly, R. K.; Wilson, J. N.; Bakbak, S.; Park, J.O.; Srinivasarao N.; Bunz, U. H. F. Facile microstructuring of organic semiconducting polymers by the breath figure method: hexagonally ordered bubble arrays in rigid rod-polymers. *Adv. Mater*. **2004**, *16*, 115-118.
37. Bolognesi A.; Mercogliano, C.; Yunus, S.; Civardi, M.; Comoretto, D.; Turturro, A. Self-organization of polystyrenes into ordered microstructured films and their replication by soft lithography. *Langmuir* **2005**, *21*, 3480-3485.
38. Zhu, L.-W.; Ou, Y.; Wan, L-S.; Xu Z.K. Polystyrenes with hydrophilic end groups: synthesis, characterization, and effects on the self-assembly of breath figure arrays. *J. Phys. Chem. B* **2014**, *118*, 845–854.
39. Amirkhani, M.; Berger, N.; Abdelmohsen, M.; Zocholl, F.; Gonçalves, M. R.; Marti, O. The effect of different stabilizers on the formation of self-assembled porous film via the breath-figure technique. *J. Polymer Sci. B* **2011**, *49*, 1430–1436.
40. Peng, J.; Han, Y.; Yang, Y.; Li, B. The influencing factors on the macroporous formation in polymer films by water droplet templating. *Polymer* **2004**, *45*, 447–452.
41. Ferrari, E.; Fabbri, P.; Pilati, F. Solvent and substrate contributions to the formation of breath figure patterns in polystyrene films. *Langmuir* **2011**, *27*, 1874–1881.
42. Liu, C.; Gao, C.; Yan, D. Honeycomb-patterned photoluminescent films fabricated by self-assembly of hyperbranched polymers. *Angewandte Chemie*, **2007**, *46*, 4128–4131.
43. Jenekhe, S. A.; Chen, X. L. Self-Assembly of ordered microporous materials from rod-coil block copolymers, *Science* **1999**, *283*, 372-375.
44. Matsuyama, H.; Ohga, K.; Maki, T.; Teramoto, M. The Effect of polymer molecular weight on the structure of a honeycomb patterned thin film prepared by solvent evaporation. *J. Chem. Eng. Japan* **2004**, *37*, 588-591.
45. Xu, Y.; Zhu, B.; Xu, Yo. A study on formation of regular honeycomb pattern in polysulfone film. *Polymer* **2005**, *46*, 713-717.
46. Bormashenko E.; Pogreb, R.; Stanevsky, O.; Bormashenko, Y.; Gendelman, O. Formation of honeycomb patterns in evaporated polymer solutions: Influence of the molecular weight. *Materials Lett*. **2005**, *59*, 3553 – 3557.
47. Li, Zh.; Ma, X.; Kong, Q.; Zang, D.; Guan, X.; Ren, X. Static and dynamic hydrophobic properties of honeycomb structured films via breath figure method. *J. Phys. Chem. C* **2016**, *120*, 18659−18664.
48. Govor, L.V.; Bashmakov, I. A.; Kiebooms, R.; Dykonov, V.; Parisi, J. Self-organized networks based on conjugated polymers. *Adv. Mater*. **2001**, *13*, 588–591.
49. Deepak, V. D.; Asha, S. K. Random and AB diblock copolymers of tricyclodecanemethanol urethane methacrylate with styrene: Synthesis and morphology characterization. *J. Polymer Sci. A* **2008**, *46* , 1278–1288.
50. Erdogan, B.; Song, L.; Wilson, J. N. Park, J. O.; Srinivasarao, M.; Bunz, U H. F. Permanent bubble arrays from a cross-linked poly(para-phenyleneethynylene): picoliter holes without microfabrication. *J. Am. Chem. Soc*. **2004**, *126*, 3678-3679
51. Karikari, A.S.; Williams, As. R.; Heisey, C. L.; Rawlett, A. M.; Lon, T. E. Porous thin films based on photo-cross-linked star-shaped Poly(d,l-lactide)s. *Langmuir* **2006**, *22*, 9687–9693.

52. Zhu, L.-W.; Yang, W.; Wan, L-S.; Xu, Z-K. Synthesis of core cross-linked star polystyrene with functional end groups and self-assemblies templated by breath figures. *Polym. Chem*. **2014**, *5*, 5175-5182.
53. Yabu, H.; Tanaka, M.; Ijiro, K.; Shimomura, M. Preparation of honeycomb-patterned polyimide films by self-organization. *Langmuir* **2003**, *19*, 6297–6300.
54. Bormashenko, Ed.; Schechter, Al.; Stanevsky, O.; Stein, T.; Balter, S.; Musin, A.; Bormashenko, Ye.; Pogreb, R.; Barkay, Z.; Aurbach, D. Free-standing, thermostable, micrometer-scale honeycomb polymer films and their properties. *Macrom. Materials & Eng*. **2008**, *293*, 872–877.
55. Bormashenko, Ed.; Balter, S.; Malkin, A.; Aurbach, D. Polysulfone membranes demonstrating asymmetric diode-like water permeability and their applications. *Macrom. Materials & Eng*. **2014**, *299*, 27–30.
56. Gong, J.; Xu, B.; Tao, X. Breath figure micromolding approach for regulating the microstructures of polymeric films for triboelectric nanogenerators. *ACS Appl. Mater. Interfaces* **2017**, *9*, 4988–4997.
57. Sharma, V.; Song, L.; Jones, R. L.; Barrow, M. S.; Williams, P.R.; Srinivasarao, M. Effect of solvent choice on breath-figure-templated assembly of "holey" polymer films. *EPL*, **2010**, *91*, 38001.
58. Bormashenko, Ed.; Pogreb, R.; Stanevsky, O.; Bormashenko, Ye.; Tamir, S.; Cohen, R. Nunberg, M.; Gaisin, V-Z.; Gorelik, M.; Gendelman, O. Mesoscopic and submicroscopic patterning in thin polymer films: Impact of the solvent. *Mater. Lett*. **2005**, *59*, 2461–2464.
59. H. Battenbo, H.; Cobley, R, J.; Wilks, S. P. A quantitative study of the formation of breath figure templated polymer materials. *Soft Matter* **2011**, *7*, 10864-10873.
60. Karthaus, O.; Maruyama, N.; Cieren, X.; Shimomura, M.; Hasegawa, H.; Hashimoto, T. Water-assisted formation of micrometer-size honeycomb patterns of polymers. *Langmuir* **2000**, *16*, 6071–6076.
61. Bormashenko, Ed. Balter, S.; Aurbach, D. On the Nature of the breath figures self-assembly in evaporated polymer solutions: revisiting physical factors governing the patterning. *Macromolecular Chem. Phys.* **2012**, *213*, 1742–1747.
62. Bormashenko, E.; Malkin, A.; Musin, A.; Bormashenko, Y.; Whyman, G.; Litvak, N.; Barkay, Z.; Machavariani, V. Mesoscopic patterning in evaporated polymer solutions: poly(ethylene glycol) and room-temperature-vulcanized polyorganosilanes/-siloxanes promote formation of honeycomb structures. *Macromol. Chem. Phys*. **2008**, *209*, 567–576.
63. Bormashenko, Ed. Correct values of Rayleigh and Marangoni numbers for liquid layers deposited on thin substrates. *Ind. Eng. Chem. Res*. **2008**, *47*, 1726–1728.
64. Hernández-Guerrero M.; Stenzel, M. H. Honeycomb structured polymer films via breath figures. *Polym. Chem*. **2012**, *3*, 563-577.
65. Nurmawati, B. M. H.; Vetrichelvan, M.; Valiyaveettil, S. Morphological investigations of self-assembled films from a pyridine -incorporated poly (p-phenylene). *J. Porous Mater*. **2006**, *13*, 315–317.
66. Maruyama, N.; Koito, T.; Nishida, J.; Sawadaishi, T.; Cieren, X.; Ijiro, K.; Karthaus, O.; Shimomura, M. Mesoscopic patterns of molecular aggregates on solid substrates. *Thin Solid Films* **1998**, *327–329*, 854.
67. Stenzel, M. H.; Barner-Kowollik, C.; Davis, T. P. Formation of honeycomb-structured, porous films via breath figures with different polymer architectures. *J. Polymer Sci. A* **2006**, *44*, 2363–2375.
68. Kabuto, T.; Hashimoto, Y.; Karthaus, O. Thermally stable and solvent resistant mesoporous honeycomb films from a crosslinkable polymer. *Adv. Funct. Mater*. **2007**, *17*, 3569–3573.
69. Sun, W.; Ji, J.; Shen, J. Rings of nanoparticle-decorated honeycomb-structured polymeric film: The Combination of Pickering emulsions and capillary flow in the breath figures method. *Langmuir* **2008**, *24* , 11338–11341.
70. Lakshmi, V.; Raju, A.; Resmi V. G.; Pancrecious, J. K.; Rajan T. P. D.; Pavithran C. Amino-functionalized breath-figure cavities in polystyrene–alumina hybrid films: effect of particle concentration and dispersion. *Phys. Chem. Chem. Phys*. **2016**, *18*, 7367-7373.
71. Wang, L-P.; Yin, K-Y.; Li, G.; Liu, Q.; Deng, A-X.; Ma, H-Y. Rhodamine B-loaded star polystyrenes and their luminescent honeycomb-patterned porous films. *Reactive & Functional Polym.* **2016**, *99*, 59–64.
72. Madej, W.; Budkowski, A.; Raczkowska, J.; Rysz, J. Breath figures in polymer and polymer blend films spin-coated in dry and humid ambience. *Langmuir* **2008**, *24*, 3517–3524.

73. Park, M. S.; Kim, J. K. Breath figure patterns prepared by spin coating in a dry environment. *Langmuir* **2004**, *20 (13)*, 5347–5352.
74. Park, M. S.; Kim, J. K. Broad-band antireflection coating at near-Infrared wavelengths by a breath figure. *Langmuir* **2005**, *21* , 11404–11408.
75. Park, M. S.; Joo, W.; Kim, J. K. Porous structures of polymer films prepared by spin coating with mixed solvents under humid condition. *Langmuir* **2006**, *22*, 4594–4598.
76. Muñoz-Bonilla, A.; Ibarboure, E.; Papon, E. Rodriguez-Hernandez, J. Self-organized hierarchical structures in polymer surfaces: self-assembled nanostructures within breath figures. *Langmuir* **2009**, *25*, 6493–6499.
77. Arora, J. S.; Cremaldi, J. C.; Hollerana M. K.; Ponnusamya, T.; Sunkaraa B.; He, J.; Pesika, N. S.; John, V. T. Hierarchical patterning of hydrogels by replica molding of impregnated breath figures leads to superoleophobicity. *Nanoscale* **2016**, *8*, 18446-18453.
78. Galeotti, Fr.; Trespidi, Fr.; Pasini, M. Breath figure-assisted fabrication of nanostructured coating on silicon surface and evaluation of its antireflection power. *J. Nanomaterials*, **2016**, *2016*, 3502310, http://dx.doi.org/10.1155/2016/3502310
79. Yabu, H.; Shimomura, M. Single-step fabrication of transparent superhydrophobic porous polymer films. *Chem. Mater*. **2005**, *17* , 5231–5234.
80. Yang, H.; Jiang, P. Self-cleaning diffractive macroporous films by doctor blade coating. *Langmuir* **2010**, *26*, 2598–12604.
81. Mansouri, J.; Yapit, E.; Chen, V. Polysulfone filtration membranes with isoporous structures prepared by a combination of dip-coating and breath figure approach. *J. Membrane Sci.* **2013**, *444*, 237–251.
82. Van-Tien Bui, V-T.; Thuy, L.T.; Tran, Q. C.; Nguyen, V-T.; Dao, V-D.; Choi J. S.; Choi, H-S. Ordered honeycomb biocompatible polymer films via a one-step solution-immersion phase separation used as a scaffold for cell cultures. *Chem. Eng. J.* **2017**, *320*, 561–569.
83. Bera, S.; Pal, M.; Sarkar, S.; Jana, S. Hierarchically structured macro with nested mesoporous zinc Indium Oxide conducting film. *ACS Appl. Mater. Interf.* **2017**, *9*, 4420–4424.
84. Yang, H.; Jiang, P. Large-scale colloidal self-assembly by doctor blade coating. *Langmuir* **2010**, *26*, 13173–13182.
85. Schmelzer, J. W. P., Schmelzer, J. Jr. Reconciling Gibbs and van der Waals: A new approach to nucleation theory, *J. Chem. Physics*, **2000**, *112*, 3820- 3831.
86. Landau L. D., Lifshitz E. M. *Statistical Physics*. Course of Theoretical Physics, V. 5, 2nd ed., Pergamon Press, Oxford, 1969.
87. Saunders, A. T.; Dickson, J. L.; Shah, P. S.; Lee, M. Y.; Lim, R. T.; Johnston, K. P.; Korgel, B. A. Breath figure templated self-assembly of porous diblock copolymer films. *Phys. Rev. E* **2006**, *73*, 031608.
88. Adamson A. W., Gast A. P. *Physical Chemistry of Surfaces*, 6th ed., Wiley, NY, 1997.
89. Lothe, J.; Pound G. M. Reconsiderations of nucleation theory. *J. Chem. Phys*. **1962**, *36*, 2080-2085.
90. Binder, R.; Stauffer, D. Statistical theory of nucleation, condensation and coagulation, *Advances in Physics*, **1976**, *25*, 343-396
91. Zeldovich, Ya. B. On the theory of formation of new phase. Cavitation, (In Russian) *J. Exptl. Theoret. Phys. USSR*, **1942**, *12*, 525-538.
92. Sigsbee, R. A. Vapor to condensed-phase heterogeneous nucleation. In: A.C. Zettlemoyer (Editor), *Nucleation*, Marcel Decker, New York, 1969, pp. 151-224.
93. Böker, A.; Lin, Y.; Chiapperini, K.; Horowitz, R.; Thompson, N.; Carreon, V.; Xu, T.; Abetz, Cl.; Skaff, H.; Dinsmore, A. D.; Emrick, T.; P. Russell, T. P. Hierarchical nanoparticle assemblies formed by decorating breath figures. *Nature Materials* **2004**, *3*, 302 – 306.
94. Escalé, P.; Rubatat. L.; Billon, L.; Save, M. Recent advances in honeycomb-structured porous polymer films prepared via breath figures. *Europ. Polymer J*. **2012**, *48*, 1001-1025.
95. Bormashenko, Ed.; Pogreb, R.; Musin, Al.; Stanevsky, O.; Bormashenko, Ye.; Whyman, G.; Gendelman, O.; Barkay, Z. Self-assembly in evaporated polymer solutions: Influence of the solution concentration. *J. Colloid & Interface Sci*. **2006**, *297*, 534-540.

96. Bormashenko, Ed.; Pogreb, R.; Stanevsky, O.; Bormashenko, Ye.; Stein, T.; Gengelman, O. Mesoscopic patterning in evaporated polymer solutions: New experimental data and physical Mechanisms. *Langmuir* **2005**, *21*, 9604–9609.
97. Bormashenko, Ed.; Whyman, G.; Pogreb, R.; Stanevsky, O.; Hakham-Itzhaq, M.; Gendelman, O. Self-assembly in evaporated polymer solutions: patterning on two scales. *Israel J. Chemistry*, **2007**, *47*, 319–328.
98. Nie1, Z, Kumacheva, E. Patterning surfaces with functional polymers. *Nature Materials* **2008**, *7*, 277 – 290.
99. Tokuhisa, H.; Tsukamoto, S.; Morita, S.; Ise, Sh.; Tomita, M.; Shirakawa, N. Fabrication of micro-textured surfaces for a high hydrophobicity by evaporative patterning using screen mesh templates. *Appl. Surf. Sci.* **2017**, *400*, 64–70.
100. Pototsky, A.; Bestehorn, M.; Merkt, D.; Thiele, U. Morphology changes in the evolution of liquid two-layer films *J. Chem. Phys*. **2005**, *122*, 224711.
101. Pototsky, A.; Bestehorn, M.; Merkt, D.; Thiele, U. Alternative pathways of dewetting for a thin liquid two-layer film. *Phys. Rev. E* **2004**, *70*, 025201(R).
102. Müller-Buschbaum, P.; Bauer, E.; Wunnicke, O.; Stamm, M. The control of thin film morphology by the interplay of dewetting, phase separation and microphase separation. *J. Phys. Condens. Matter* **2005**, *17*, S363.
103. Colinet, P.; Legros, J. C.; Velarde, M. G. *Nonlinear Dynamics of Surface–Tension–Driven Instabilities*, Wiley, Berlin, 2001.
104. Nepomnyashchy, A.A.; Velarde, M. G.; Colinet, P.; *Interfacial Phenomena and Convection*, Chapman & Hall/CRC, 2002, Boca Raton, USA.
105. Reichenbach, J.; Linde, H. Linear perturbation analysis of surface-tension-driven convection at a plane interface (Marangoni instability). *J. Colloid Interface Sci*. **1981**, *84*, 433-443.
106. Linde, H.; Velarde, M.G.; Wierschem, A.; Waldhelm, W.; Loeschke, K.; Rednikov, A. Y. Interfacial wave motions due to Marangoni instability. *J. Colloid Interface Sci*. **1997**, *188*, 16-26.
107. Oron, A.; Nepomnyashchy, A.A. Long-wavelength thermocapillary instability with the Soret effect, Phys. Rev. E **2004**, *69*, 016313.
108. Regnier, V.C.; Dauby, P.C.; Lebon, G. Linear and nonlinear Rayleigh–Bénard–Marangoni instability with surface deformations. *Phys. Fluids* **2000**, *12* **,** 2787.
109. Zhang, N.; Chao, D. F. Mechanisms of convection instability in thin liquid layers induced by evaporation. *Int. Commun. Heat Mass Transfer* **1999**, *26*, 1069-1080.
110. Münch, A.; Please, C. P.; Wagner, B. Spin coating of an evaporating polymer solution. *Phys. Fluids* **2011**, *23*, 102101.
111. Mitov, Z.; Kumacheva, E. Convection-induced patterns in phase-separating polymeric fluids. *Phys. Rev. Lett*. **1998**, *81*, 3427.
112. Minařík, A.; Smolka, P.; Minařík, M.; Mráček, A.; Rajnohová, E.; Minaříková, M.; Gřundělová, L.; Foglarová, M. ; Velebný Vl. A special instrument for the defined modification of polymer properties in solutions and polymer layers. *Measurement* **2017**, *97*, 218–225.
113. Wrzecionko, E.; Minařík, A.; Smolka, P.; Minařík, M.; Humpolíček, P.; Rejmontová, P.; Mráček, A.; Minaříková, M.; Gřundělová, L. Variations of polymer porous surface structures via the time-sequenced dosing of mixed solvents. *ACS Appl. Mater. Interfaces* **2017**, *9*, 6472–6481.
114. Fowler, P. D.; Ruscher, C.; McGraw, J. D.; Forrest, J. A.; Dalnoki-Veress, K. Controlling Marangoni-induced instabilities in spin-cast polymer films: How to prepare uniform films. *European Phys. J. E* **2016**, *39*, 90.
115. Bormashenko, Ed.; Balter, S.; Pogreb, R.; Bormashenko, Ye.; Gendelman, O.; Aurbach, D. On the mechanism of patterning in rapidly evaporated polymer solutions: Is temperature-gradient-driven Marangoni instability responsible for the large-scale patterning? *J Colloid & Interface Sci*. **2010**, *343*, 602-607.
116. Grigoriev, R. Control of evaporatively driven instabilities of thin liquid films. *Phys. Fluids*, **2002**, *14*, 1895.

117. P.G. De Gennes, P. G. Instabilities during the evaporation of a film: Non-glassy polymer + volatile solvent *Eur. Phys. J. E* **2001,** *6*, 421-424.
118. De Gennes, P. G. Solvent evaporation of spin cast films: "crust" effects. *Eur. Phys. J. E* **2002**, *7*, 31-34.
119. Bormashenko, Ed. Surface instabilities and patterning at liquid/vapor interfaces: Exemplifications of the "hairy ball theorem". *Colloids & Interface Sci. Comm.* **2015**, *5*, 5-7.
120. Eisenberg, M.; Guy, R. A proof of the hairy ball theorem. *American Mathematical Monthly*, **1979**, *86*, 571-574.
121. Bormashenko, Ed.; Aurbach. D.; Whyman, G.; Stein, T.; Bormashenko, Ye.; Pogreb, R. On the role of the Plateau borders in the pattern formation occurring in thin evaporated polymer layers. *Colloids & Surfaces A*, **2008**, *312*, 245-248.
122. Park, S. H.; Xia, Y. Macroporous membranes with highly ordered and three-dimensionally interconnected spherical pores. *Adv. Mater*. **1998**, *10*, 1045–1048.
123. Zhang, Y.; Wang, C. Micropatterning of proteins on 3D porous polymer film fabricated by using the breath-figure method. *Adv. Mater.* **2007**, *19*, 913–916.
124. Dong, R.; Yan, J.; Ma, H.; Fang Y.; Hao, J. Dimensional architecture of Ferrocenyl-based oligomer honeycomb-patterned Films: From monolayer to multilayer. *Langmuir* **2011**, *20*, 9052–9056.
125. Kralchevsky, P. A.; Danov, K. D.; Denkov N. D. Chemical physics of colloid systems and interfaces, Chapter 5 in *Surface and Colloidal Chemistry*, Ed. by K.S. Birdi, CRC Press, Boca Raton, 2003.
126. Kralchevsky, P. A.; Nagayama, K. Capillary forces between colloidal particles. *Langmuir* **1994**, *10*, 23–36.
127. Kralchevsky, P. A., Nagayama, K. Capillary interactions between particles bound to interfaces, liquid films and biomembranes. *Adv. Colloid & Interface Sci.* **2000**, *85*, 145–192.
128. Kralchevsky, P. A.; Paunov, V. N.; Ivanov, I. B., Nagayama, K. Capillary meniscus interactions between colloidal particles attached to a liquid-fluid interface. *J. Colloid & Interface Sci.* **1992**, *151*, 79-94.
129. Bragg, L.; Nye, J. F. A dynamical model of a crystal structure. *Proceedings of the Royal Society of London A* **1947**, *190*, 474-481.
130. Lomer, W. M. The forces between floating bubbles and a quantitative study of the Bragg "Bubble Model" of a crystal. *Mathematical Proceedings of the Cambridge Philosophical Soc.* **1949**, *45*, 660 – 673.
131. Peiranski, P. Two-Dimensional interfacial colloidal crystals. *Phys. Rev. Lett*.**1980**, *45*, 569-573.
132. Dong, R.; Ma, H.; Yan, J.; Fang, Y.; Hao, J. Tunable morphology of 2D honeycomb-patterned films and the hydrophobicity of a Ferrocenyl-based oligomer. *Chemistry Europ. J*. **2011**, *17*, 7674–7684
133. Dou, Y.; Jin, M.; Zhou, G.; Shui, L. Breath figure method for construction of honeycomb films. *Membranes* **2015**, *5*, 399-424.
134. Tadmor, R. Line energy and the relation between advancing, receding and Young contact angles. *Langmuir* **2004**, *20*, 7659-7664.
135. Xia, Y.; Gates, B.; Yin, Y.; Sun, Y. Self-assembly of monodispersed spherical colloids into complex structures, in Surface and Colloid Chemistry, 2nd ed. Edited by K.S. Birdy, CRC press, 2003, Boca Raton, USA, pp. 555-579
136. Yin, Y.; Xia, Y. Self-assembly of monodispersed colloidal spheres into complex aggregates with well-defined sized, shapes and structures. *Adv. Mater*. **2001**, *13*, 267.
137. De León, A. S.; Malhotra, S.; Molina, M.; Haag, R.; Calderón, M.; Rodríguez-Hernández, J.; Muñoz-Bonilla, A. Dendritic amphiphiles as additives for honeycomb-like patterned surfaces by breath figures: Role of the molecular characteristics on the pore morphology. *J. Colloid 7 Interface Sci*. **2015**, *440*, 263-271.
138. Wu, Ch-H.; Ting, W-H.; Lai, Y-W.; Dai, S. A.; Su, W-C.; Tung, Sh-H.; Jeng, R. J. Tailored honeycomb-like polymeric films based on amphiphilic poly(urea/malonamide) dendrons.
RSC Adv. **2016**, *6*, 91981-91990.
139. Fedorets, A. A. On the mechanism of non-coalescence in a drop cluster. *JETP Lett*. **2005**, *81*, 437–441.
140. Fedorets, A. A.; Dombrovsky, L. A.; Smirnov, A. M. The use of infrared self-emission measurements to retrieve surface temperature of levitating water droplets. *Infrared Physics & Techn.* **2015**, *69*, 238–243.

141. Fedorets, A. A.; Frenkel, M.; Shulzinger, E.; Dombrovsky, L. A.; Bormashenko, Ed.; Nosonovsky, M. Self-assembled levitating clusters of water droplets: pattern formation and stability. *Sci. Rep*. **2017**, *7*, 1888.
142. Eggers, J.; Lister, J. R.; Stone H. A. Coalescence of liquid drops. *J. Fluid Mech*. **1999**, *401*, 293-310.
143. Aarts, D. G. A. L.; Lekkerkerker, H. N. W.; Guo, H.; Wegdam, G. H.; Bonn, D. Hydrodynamics of droplet coalescence. *Phys. Rev. Lett*. **2005**, *95*, 164503.
144. Karpitschka, S.; Riegler, H. Sharp transition between coalescence and non-coalescence of sessile drops. *J. Fluid Mech*. **2014**, 743, R1.
145. Karpitschka, S.; Riegler, H. Quantitative experimental study on the transition between fast and delayed coalescence of sessile droplets with different but completely miscible liquid. *Langmuir* **2010**, *26*, 11823–11829.
146. Karpitschka, S.; Riegler, H. Noncoalescence of sessile drops from different but miscible liquids: hydrodynamic analysis of the twin drop contour as a self-stabilizing traveling wave. *Phys. Rev. Lett*. **2012**, *109*, 066103.
147. Ma, H.; Hao, J. Evaporation-induced ordered honeycomb structures of gold nanoparticles at the air/water interface. *Chem. - Eur. J*. **2010**, *16*, 655−660.
148. Li, J.; Peng, J.; Huang, W. H.; Wu, Y.; Fu, J.; Cong, Y.; Xue, L. J.; Han, Y. C. Ordered honeycomb-structured gold nanoparticle films with changeable pore morphology: from circle to ellipse. *Langmuir* **2005**, *21*, 2017−2021.
149. Saito, Y.; Shimomura, M.; Yabu, H. Breath figures of nanoscale bricks: a universal method for creating hierarchic porous materials from inorganic nanoparticles stabilized with mussel-inspired copolymers. *Macromol. Rapid Commun*. **2014**, *35*, 1763−1769.
150. Saunders, A. E.; Shah, P. S.; Sigman, M. B.; Hanrath, T.; Hwang, H. S.; Lim, K. T.; Johnston, K. P.; Korgel, B. A. Inverse opal nanocrystal superlattice films. *Nano Lett*. **2004**, *4*, 1943−1948.
151. Escalé, P.; Save, M; Billon, L.; Ruokolainen, J.; Rubatat, L. When block copolymer self-assembly in hierarchically ordered honeycomb films depicts the breath figure process. *Soft Matter* **2016**, *12*, 790-797.
152. Roe, B. P. *Probability and Statistics in Experimental Physics*, Springer, New York, 2001.
153. Kumar, V. S.; Kumaran, V. Voronoi cell volume distribution and configurational entropy of hard-spheres. *J. Chem. Physics* **2005**, *123*, 114501.
154. Barthélemy, M. Spatial networks, *Physics Reports* **2011**, *499*, 1–101.
155. Limaye, A. V.; Narhe, R. D.; Dhote, A. M.; Ogale, S. B. Evidence for convective effects in breath figure formation on volatile fluid surfaces. *Phys. Rev. Lett*. **1996**, *76*, 3762-3765.
156. Bormashenko E., Musin A., Whyman G., Barkay Z., Zinigrad M. Revisiting the fine structure of the triple line, *Langmuir* **2013**, *29*, 14163−14167.
157. Marmur A. A guide to the equilibrium contact angles maze, in *Contact Angle Wettability and Adhesion*, V. 6, pp.3-18, ed. by K. L. Mittal, Brill/VSP, Leiden, 2009.
158. Zhou, Y.; Huang, J.; Sun, W.; Ju, Y.; Yang, P.; Ding, L.; Chen, Z-R.; Kornfield, J. A. Fabrication of active surfaces with metastable microgel layers formed during breath figure templating. *ACS Appl. Mater. Interfaces* **2017**, *9*, 4177–4183.
159. Male, U.; Shina, B. K.; Huh, D. S. Coupling of breath figure method with interfacial polymerization: Bottom-surface functionalized honeycomb-patterned porous films. *Polymer* **2017**, *119*, 206–211.
160. Bormashenko, Ed.; Bormashenko, Ye.; Pogreb, R.; Stanevsky, O. Micrometrically scaled textured metallic hydrophobic interfaces validate the Cassie–Baxter wetting hypothesis. *J. Colloid & Interface Sci*. **2006**, *302*, 308-311.
161. Yabu, H.; Takebayashi, M.; Tanaka, M.; Shimomura, M. Superhydrophobic and lipophobic Properties of self-organized honeycomb and pincushion structures. *Langmuir* **2005**, *21*, 3235–3237.
162. Cassie, A. B. D.; Baxter, S., Wettability of porous surfaces. *Trans. Faraday Soc*. **1944**, *40*, 546 – 551.
163. Cassie, A. B. D. Contact angles. *Discuss. Faraday Soc*. **1948**, *3*, 11 – 16.
164. Nosonovsky, N.; Bhushan, B. Superhydrophobic surfaces and emerging applications: Non-adhesion, energy, green engineering. *Current Opinion Colloid & Interface Sci*. **2009**, *14*, 270-280.

165. Nosonovsky, N.; Bhushan, B. Biologically inspired surfaces: Broadening the scope of roughness. *Advanced Functional Mater.* **2008**, *18* (6), 843-855.
166. Whyman, G.; Bormashenko, Ed. How to make the Cassie wetting state stable? *Langmuir* **2011**, *27*, 871-8176.
167. Arinstein, A.; Burman, M.; Gendelman, O.; Zussman, E. Effect of supramolecular structure on polymer nanofibre elasticity. *Nature nanotechnology* **2007,** *2*, 59-62.
168. Martínez-Campos, E.; Elzein, T.; Bejjani, A.; García-Granda, M. J.; Santos-Coquillat, A.; Ramos, V.; Muñoz-Bonilla, A.; Rodríguez-Hernández, J. Toward cell selective surfaces: cell adhesion and proliferation on breath figures with antifouling surface chemistry. *ACS Appl. Mater. Interfaces* **2016**, *8*, 6344–6353.
169. Gong, J.; Xu, B.; Tao, X.; Li, L. Binary breath figures for straightforward and controllable self-assembly of microspherical caps. *Phys. Chem. Chem. Phys*. **2016**, *18*, 13629-13637.
170. Abbaspour, M.; Pourabbas, B.; Azimi, M. Solid-state supercapacitor based on breath figured polymethyl methacrylate deposited by graphene: the effect of electrode surface. *J Mater Sci: Mater Electron.* **2017**, doi:10.1007/s10854-017-7265-z
171. Bormashenko, Ed.; Pogreb, R.; Balter, S.; Aurbach, D. Electrically controlled membranes exploiting Cassie-Wenzel wetting transitions. *Scientific Reports* **2013**, *3*. 3028.